Search Coil-based Detection of Non-adjacent Rotor Bar Damage in Squirrel Cage Induction Motors

Search Coil-based Detection of Non-adjacent Rotor Bar Damage in Squirrel Cage Induction Motors

Yonghyun Park*, Hanchun Choi*, Sang Bin Lee* and Konstantinos Gyftakis**
*Korea University, Seoul, Korea
**University of Edinburgh, Edinburgh, UK

***Abstract*—Detection of rotor cage faults in induction motors based on motor current signature analysis (MCSA) is being extensively applied in the field for preventing forced outage of the motor and industrial process. Although MCSA is very effective for detecting broken bars that are adjacent to each other, it can fail if the broken bars are non-adjacent, which is common for applications with frequent starts. If multiple broken bars are spread out at locations where the rotor "electrical" asymmetry is canceled, the presence of broken bars is difficult to detect with MCSA. A false indication can lead to a catastrophic forced outage, but the only known means of detecting this type of fault in the field is through rotor visual inspection. In this paper, the feasibility of detecting non-adjacent broken rotor bars from the rotor rotational frequency sideband components in the internal and external search coil measurements during steady state and motor starting is evaluated. Experimental testing on a 7.5 hp induction motor shows that non-adjacent broken bars can be reliably detected from the analysis of flux measurements for cases where MCSA and all other electrical tests fail.**

***Index Terms*—Airgap Flux, Fault Diagnostics, Induction Motor, Off-line Testing, Search Coil, Squirrel Cage Rotor, Spectral Analysis, Starting Transient, Stray Flux.**

I. Introduction

Faults in the squirrel cage rotor of induction motors is known to be common for applications with frequent start/stops and large load variations. Induction motors with rotor faults will continue to operate, but it is important to detect and repair broken rotor bars in medium-high voltage induction machines to prevent secondary damage caused by the fault. Arcing between the loose broken bar and rotor core can result in permanent core damage and also pose a safety risk in explosive environments. Moreover, loose broken bars (or fragments) can protrude into the stator core or endwinding and cause forced outage of the motor and driven process [1]-[6]. Many off-line tests and on-line monitoring methods have been developed over the years to detect rotor faults to prevent additional damage to the motor [3]-[5].

Among the rotor monitoring methods available, MCSA is the most popular test employed in the field since it can provide remote, on-line monitoring of rotor faults using the current measurement available in the motor control center (MCC). Although MCSA has been successful in detecting rotor cage faults, many cases of false positive (false alarm) and negative (missed fault) indications produced due to the influence of rotor structural asymmetry or load/operating conditions have been reported [6]-[14], as summarized in Table I. There has been active research on alternative test methods immune to false indications to improve the reliability of rotor fault detection [10]-[16]. It has been shown in [6], [10]-[13] that testing the motor when the rotor slip is high (such as standstill or starting transient) is immune to most of the false indications, as highlighted in Table I.

Rotor bars usually break in the rotor bar overhang area where the thermo-mechanical stress in the bars is highest [1]-[2]. It is common for bars adjacent to the damaged bars to break because current is redistributed to neighboring bars increasing the operating stresses. However, cases of non-adjacent broken bars are also observed for applications with frequent transient stresses [6]. Examples of non-adjacent broken bars that have been observed by the authors are shown in Fig. 1 for 6.6 kV, 500 kW, 10 pole coal crusher, and 380 V, 190 kW, 4 pole fuel pump induction motors. The end rings cut off from the rotor cage clearly shows that bar breakages can be randomly spread out. MCSA based on monitoring the 2x slip frequency sidebands of the fundamental frequency, f_s,

$$f_{brb} = (1 \pm 2ks) \cdot f_s, \tag{1}$$

Table I. Root causes of false positive and negative rotor fault indications produced by MCSA. False indications immune to testing under high rotor slip (standstill or starting transient) are highlighted.

Actual rotor condition	Diagnosis of MCSA: Healthy	Diagnosis of MCSA: Faulty
Healthy	True Negative	False Positive • Low frequency load oscillations • Axial air duct • Magnetic anisotropy • Impellers/cylinders • Rotor ovality • Porosity (*Al* die cast rotor)
Faulty	False Negative • Outer cage fault in double cage rotor • Nonadjacent broken bars • Load variation • Incorrect speed estimate	True Positive

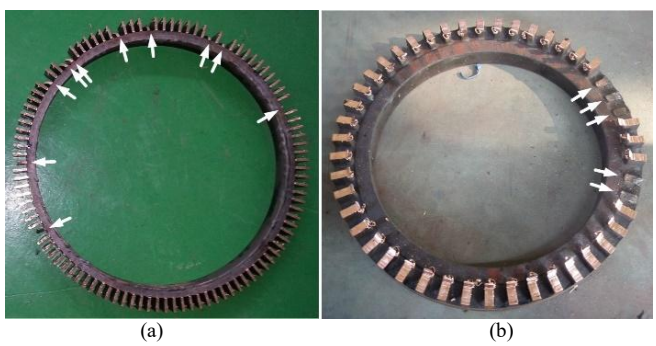

(a) (b)

Fig. 1. Examples of non-adjacent broken bars: end ring of (a) 6.6 kV, 500 kW, 10 pole coal crusher and (b) 380 V, 190 kW, 4 pole fuel pump induction motors with location of broken bars shown.

is very effective for detecting adjacent broken bars (k is an integer, and s is the rotor slip). However, it has been shown in [7], [14]-[20] that rotor faults are difficult to detect if the location of non-adjacent broken bars is such that the electrical asymmetry of the rotor observed from the stator winding is canceled. For example, the electrical asymmetry seen from the stator is canceled if 2 broken bars are separated by 90° (electrical) or half pole pitch (or if 3 broken bars are separated by 120° (electrical), etc…). Therefore, it is likely for the f_{brb} component to be significantly reduced and not proportional to the number of broken bars, if the bars are spread out as in the cases of Fig. 1. This causes MCSA based on f_{brb} to produce a false negative indication where the fault cannot be observed, and potentially lead to a forced outage without prior warning.

All commercial electrical tests including MCSA, single phase rotation test, and starting current analysis rely on indirectly observing the electrical asymmetry produced by broken bars from the stator winding. Therefore, they cannot detect non-adjacent broken bars that interact to cancel the electrical asymmetry [6]-[7], [14]-[20]. Since the only reliable means of detecting non-adjacent broken bars in the field is through direct visual inspection of the rotor, alternative test methods for detecting non-adjacent broken bars have been studied in [14]-[16], [19]-[22]. In [14]-[15], [23], it was shown that the 5th and 7th space harmonics-induced rotor fault components in the stator current or radial stray flux spectra can serve as reliable indicators of non-adjacent broken bars. However, it is difficult to define a fault threshold for these components since the increase with faults is small and depends on the winding factor. In [16], it is shown that non-adjacent broken bars separated by half pole pitch result in secondary local saturation in the rotor and produce $4sf_s$ sidebands in the stator current spectrum. However, it is shown in this paper that these proposed saturation-related components are not always present. The $2sf_s$ sidebands of the 3rd harmonics of the zero sequence current [21], and the $2sf_s$ sidebands of the 6th harmonics of the Park's vector [22] are proposed for detecting non-adjacent broken bars based on empirical observations. However, [21] can only be applied to delta connected motors with current measurement at the motor terminals, and it is difficult to determine the fault threshold [21]-[22]. In [24], it is shown that the sf_s component in the radial stray flux during motor starting can be used to detect non-adjacent broken bars for cases where MCSA fails. However, the sf_s component can also change with unbalance in the voltage supply and with other types of asymmetry in the machine [25]-[28]. The methods proposed in [14]-[16],[21]-[24] are yet to be verified or accepted in the field.

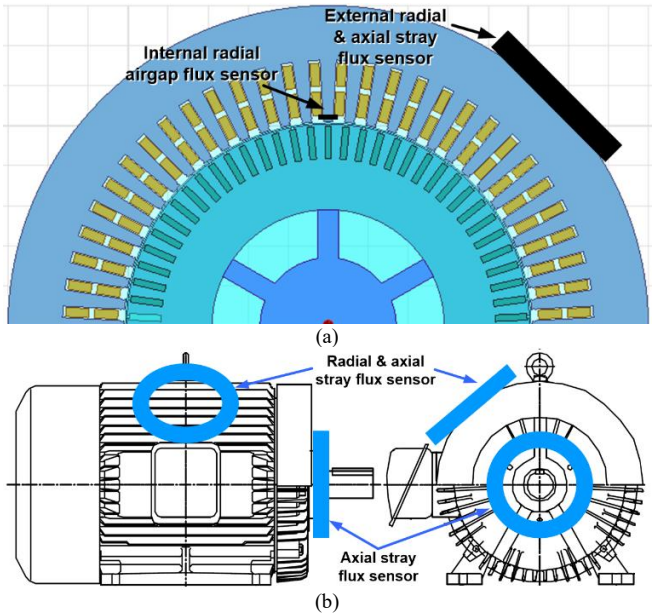

Fig. 2. Flux measurements used for motor condition monitoring: internal radial airgap flux (a); external radial and axial stray flux (a)-(b); external axial stray flux (b) measurement.

In this work, the feasibility of using internal and external search coil measurements are investigated for providing reliable detection of non-adjacent broken rotor bars under motor starting and steady state operation. The rotor rotational frequency sideband components of f_s in the flux signals are proposed as reliable indicators for supporting MCSA to detect non-adjacent broken bars. A theoretical analysis and experimental testing on a 7.5 hp induction motor under controlled non-adjacent broken bar conditions clearly show that the proposed fault indicators can reliably detect rotor faults for cases where MCSA and other electrical tests fail.

II. Airgap and Stray Flux Monitoring

The concept of using flux measurements for detecting faults in electric machines has been studied since the 70s due to its potential benefits in terms of cost, simplicity, and flexibility. Analysis of external stray flux and internal airgap flux have been applied for detecting rotor conductor, eccentricity, stator winding/core, bearing faults, and supply unbalance for ac machines [5], [23]-[41]. It is claimed in [28]-[30] that flux analysis can provide detection of rotor faults with sensitivity comparable or superior to current, internal flux, or vibration analysis. External flux sensors can be easily retrofit onto the surface of the motor frame for measurement of the axial and/or radial stray flux, as shown in Fig. 2. The internal flux sensors can be installed on the stator inner surface or around the stator tooth to measure the airgap flux, as shown in Fig. 2(a).

Despite the potential advantages of flux-based motor fault detection, it has not been as well-received as MCSA in the field or academia. This is mainly due to the requirement of flux sensor installation on the frame or inside the motor, which requires physical access to the motor. The remote monitoring capability with existing current sensors in the MCC is an attractive feature of MCSA, especially if large quantity of motors are operating in a hostile environment. However, there has been a recent trend where motor manufacturers are providing self-diagnostics capability through integrated sensors in the motor for technological differentiation in the competitive global market [42]-[43]. The limitations of current, vibration, and thermal sensors in terms of the reliability and diversity of fault detection have been identified, and flux monitoring is being actively investigated as a low cost option for providing additional fault information to complement existing technology. Thermal sensors are installed inside most medium-high voltage motors for monitoring the stator or bearing temperature, and accelerometers or proximity sensors are also being installed on

the important motors. Considering that the cost of installation of search coils for flux measurement is lower than that of thermal or mechanical sensors, search coil based monitoring can be justified if it can provide advanced warning of failure, especially for cases where MCSA or other tests fail. The reliability of fault detection is considered more important than convenience or remote monitoring capability due to the potentially fatal consequences of false indications.

The prior work on flux monitoring focus on exploring the detectability of faults, and on the sensitivity compared to existing technology [25]-[38]. There are only a few studies that focus on the reliability aspects of flux based monitoring, and investigate how the reliability of MCSA can be improved [23]-[24], [39]-[41], [44]. It is shown that external stray flux monitoring can provide reliable detection of rotor faults immune to the interference from low frequency load torque oscillations in [39]-[40] and magnetic rotor asymmetry in [41]. Although commercial test methods immune to interference from load torque oscillations or magnetic asymmetry are available, as presented in [6], [10]-[13], there are no known tests for reliable detection of non-adjacent broken bars. Detection of non-adjacent broken bars from the rotor rotational frequency components in the flux measurements during steady state and motor starting are investigated in the following sections.

III. Flux-based Detection of Non-adjacent Broken Rotor Bars

A. External Stray Flux

The external search coil can be placed on the radial or axial surface of the motor frame, as shown in Fig. 2. If the sensor is placed on the radial surface, the stray flux in the axial and radial direction can be measured [33]-[35]. If the sensor is placed on the axial end surface to enclose the shaft, as shown in Fig. 2(b), the axial stray flux can be measured [37]-[39]. In this work, the search coil on the radial surface is considered, since it is possible to measure both axial and radial stray flux, and also because it is difficult to install the sensor on the axial surface around the shaft for many applications.

The influence of broken rotor bars can be observed in the stray flux components in both the axial and radial direction. The 1x and 3x slip frequency components,

$$s \cdot f_s, \quad 3s \cdot f_s, \tag{2}$$

in the "axial" stray flux increase with broken bars, and have been proposed as indicators for detecting rotor faults in [24], [33]-[34]. The slip frequency, sf_s, component in the axial flux is produced by the current in the rotor end ring. Any type of asymmetry in the rotor structure directs the end ring current-induced axial flux through the shaft producing the sf_s component, which can be measured with the flux sensors shown in Fig. 2(b) [25]. The modulation of sf_s by the twice slip frequency, $2sf_s$, torque oscillation produced by the rotor fault induces $-sf_s$ and $3sf_s$ components in the axial stray flux, even for cases of non-adjacent broken bars [24]. However, considering how the low frequency components are induced, they are small in magnitude and depend on the physical structure and magnetic properties of the motor components. The inherent magnitude and increase in the sf_s component (and consequently the $3sf_s$ component) are also influenced by other asymmetries in the rotor, and supply voltage or unbalance level making it difficult to determine the fault threshold. Therefore, it may not be applicable to all motors, as will be demonstrated in the test results in IV.B.

Broken rotor bars can also be observed in the "radial" stray flux components. The $2sf_s$ sideband components, f_{brb}, shown in (1) and the space harmonics induced rotor fault components,

$$(5-4s)\cdot f_s,\ (5-6s)\cdot f_s, (7-6s)\cdot f_s,\ (7-8s)\cdot f_s, \tag{3}$$

are induced in the radial flux. However, the f_{brb} component in the stray flux is not capable of detecting non-adjacent broken bars that do not produce electrical asymmetry, since it cannot be observed in the stator current. The space harmonics-induced components in the radial stray flux increase with non-adjacent broken bars [23], as in MCSA. However, the magnitude of the components are small, and they depend on the magnitude of the space harmonics determined by the winding factor, which is usually unknown. This makes it difficult to determine the fault threshold as it is different for every motor.

Given the limitations of the aforementioned axial and radial stray flux frequency components (1)-(3), monitoring of the rotor rotational frequency, f_r, components given by

$$f_r = (1-s)\cdot f_s/p, \tag{4}$$

is considered for reliable monitoring of adjacent and non-adjacent rotor faults (p is the number of pole pairs). The waveform of the voltage, v_{coil}, of the search coil installed on the radial surface of a 7.5 hp, 4 pole motor with 2 of 44 adjacent broken bars is shown in Fig. 3. v_{coil} is the derivative of the stray flux linkage through the search coil. A broken bar in the rotor produces a radial rotating asymmetry in the airgap flux, since the rotor current is absent in the slot with the broken bar. Therefore, the effect of the rotor fault can be observed whenever the rotor slot with the broken bar passes the search coil. As a result, the rotor rotational frequency f_r that represents "once per rotor revolution" or "1x" given by (4) is reflected in the search coil voltage. The fundamental and odd harmonic components $k_{odd}f_s$ is modulated by integer multiples of f_r and induces f_r sidebands in v_{coil} given by

$$f_{rrf} = k_{odd}\cdot f_s \pm k\cdot f_r = (k_{odd} \pm k\cdot(1-s)/p)\cdot f_s, \tag{5}$$

where k_{odd} is a positive odd integer. Fluctuation in the v_{coil}

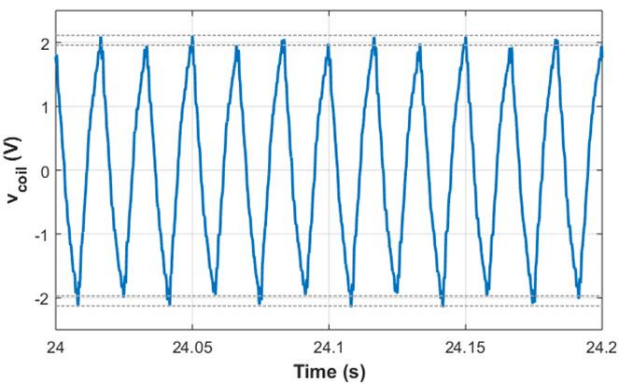

Fig. 3. Measured waveform of external stray flux terminal voltage, v_{coil}, from 7.5 hp, 4 pole induction motor with 2 of 44 adjacent broken bars.

waveform in Fig. 3 at approximately once per every two cycles can be visually observed in the time domain. This is due to the f_s-f_r (≈30 Hz) component produced by the once per revolution fluctuation of flux due to broken bars in the 4 pole motor. The integer multiples of the f_r sidebands of the supply voltage odd harmonics shown in (5) can be clearly seen in the frequency domain plot of v_{coil} shown in Fig. 4.

Although the principle of MCSA and radial stray flux spectrum analysis are identical in that the influence of the asymmetry in the motor flux is detected by a "coil", the spectra of the two signals are completely different. The symmetrical arrangement of the stator coils is such that it picks up the rotor asymmetry 2p times per revolution as the rotor passes the stator coils, making f_{brb} independent of number of pole pairs. On the other hand, the flux coil placed asymmetrically on one side of the motor picks up the rotor asymmetry once per revolution, making the induced f_{rrf} component pole-dependent. Therefore, if the non-adjacent broken bars are located such that the electrical asymmetry is canceled, it cannot be detected with the symmetrical stator windings. However, since each broken bar induces its own f_{rrf} component in the search coil, multiples of the f_r sidebands will be produced regardless of the relative location of broken bars. Therefore, non-adjacent broken bars can be detected from the f_{rrf} component of the radial stray flux.

B. Internal Radial Airgap Flux

When the airgap flux is measured through an internal flux sensor, the radial flux components that are produced by the stator current shown in (1), (3), and (5) are observable. However, the axial stray flux components, sf_s and $3sf_s$, shown in (2) cannot be observed in the airgap flux. The influence of the once per revolution mechanical asymmetry shown in (5) is more prevalent in the airgap flux compared to external flux sensors, since the airgap flux is measured in the stator inner surface close to the rotor surface. Therefore, the f_{rrf} component in (5) can be used to detect broken bars regardless of whether they are adjacent or non-adjacent, as in the case of external stray flux sensors, but with higher sensitivity. If the airgap flux is estimated from the mathematical model, it is calculated from the stator current, and is different from that of the measured flux. Analyzing the spectrum of the airgap flux estimate would have the same limitations as MCSA for this reason.

The sensitivity of fault detection can be improved further, if the f_{rrf} components are monitored during the motor starting transient. The difference in the current between healthy and faulty slots is more pronounced during rotor acceleration since the rotor current is maximum. The steep drop in the current in the slots with broken bars makes the integer multiples of the f_r sidebands in (5) more noticeable and easily detectable. The f_r sidebands will be produced for each individual broken bar, and broken bars can be detected regardless of their relative position. Therefore, the integer multiples of f_r sidebands of k_{odd}·f_s shown in (5) can be monitored during the starting transient to detect broken rotor bars whether they are adjacent or non-adjacent. It has been shown in [38] that the f_r sidebands can be observed in the airgap flux at motor starting with high sensitivity, if broken damper bars are present in salient pole synchronous motors.

The airgap flux measured from a stator tooth search coil, v_{coil}, on a 7.5 hp, 4 pole induction motor during the starting transient is shown in Fig. 5. There are many different frequency components in the waveform in addition to f_s such as f_{rrf} and rotor slot harmonics, etc, making it difficult to observe the fault related component in the time domain. What makes extraction of the f_{rrf} components more difficult is that the frequency changes during motor starting as s decreases from 1 to 0, as can be seen in (5). The variation in the f_{rrf} components are illustrated in Fig. 6 from (5) for a 4 pole induction motor for k

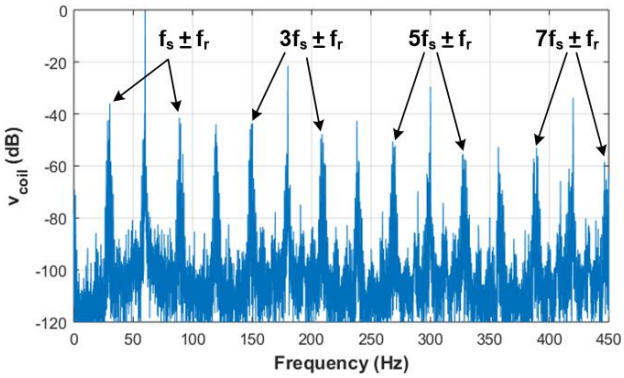

Fig. 4. Frequency spectrum of external stray flux terminal voltage, v_{coil}, from 7.5 hp, 4 pole induction motor with 2 of 44 adjacent broken bars.

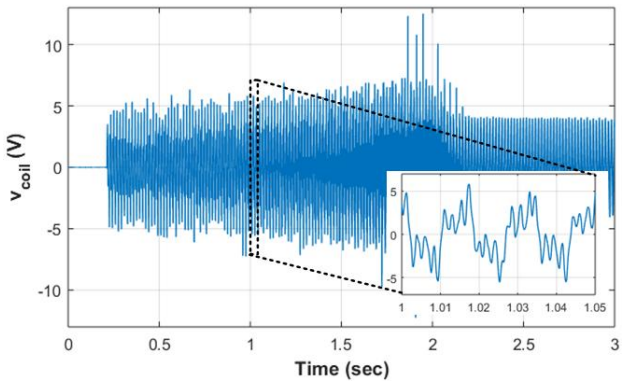

Fig. 5. Internal airgap flux terminal voltage, v_{coil}, measured during starting transient from 7.5 hp, 4 pole induction motor with 2 of 44 adjacent broken bars.

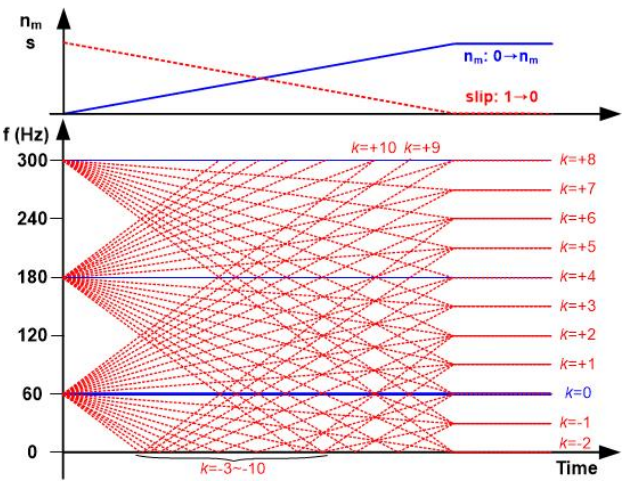

Fig. 6. Time-frequency representation of f_{rrf} components during starting of 4 pole motor as rotor accelerates to steady state (-10≤k≤+10 sidebands of k_{odd}·f_s shown for k_{odd} = 1, 3, and 5 for s: 1→0).

up to ±10. The conventional Fourier transform cannot be applied to analyze the f_{rrf} components of this non-stationary v_{coil} signal, and a suitable time-frequency analysis technique is required [45]. In this work, the short time Fourier transform (STFT) is applied to process the v_{coil} signal as it is relatively simple and has been verified to provide reliable starting transient analysis [3], [38], [45]. From the STFT time frequency plot, the $k{\cdot}f_r$ sideband components shown in red dotted lines in Fig. 6 can be monitored during the starting transient to detect broken bars whether they are adjacent or non-adjacent.

The f_{rrf} components are known to be produced by other types of faults in the motor, coupling, and load such as airgap eccentricity, load unbalance, misalignment, and other mechanical defects. Eccentricity and broken bar faults can be easily distinguished with MCSA since they produce fault components at different frequencies in steady state. Most defects in the load or coupling give rise to f_{rrf} components in the current, but the internal or airgap flux measurements are insensitive to these defects. This is because rotor faults and eccentricity distort the flux and have a direct influence on the search coils installed on the rotor, whereas load or coupling defects are indirect, as will be demonstrated in the test results.

IV. Experimental Results

A. Experimental Test Setup

The proposed search coil based detection methods were verified on a 380 V, 7.5 hp, 4 pole induction motor. The radial and axial components of the stray flux were measured with a 320 turn search coil on the frame outer surface, as shown in Fig. 7(a). The internal airgap flux was measured with a 10 turn search coil wound around a stator tooth and placed on the slot wedges, as shown in Fig. 7(b). The single phase rotation test, MCSA, and the proposed f_{rrf} based flux monitoring were performed for 4 cases of rotor faults: (a) 0, (b) 1, and (c) 2 adjacent broken bars, and (d) 2 non-adjacent broken bars 90° electrical (45° mechanical) apart. Broken bar conditions were emulated by separating the bar and end ring. The motors were started directly from the line, and loaded with a magnetic brake to operate between 0.83~1% slip. The stator current, external and internal airgap flux, and acceleration were acquired with a commercial data acquisition system at 6 kHz during motor starting and steady state operation.

B. Experimental Results

The results of the off-line single phase rotation test [4]-[5] performed with 45 V applied between two phases with the rotor rotated in 10° steps, are shown in Fig. 8 for the 4 rotors. It can be seen that the fluctuation in the normalized current, I_{rms}, increases for 0, 1, 2 adjacent broken bars since the asymmetry increases with the number of broken bars. However, for the case of 2 non-adjacent broken bars separated by 90° (electrical), the I_{rms} measurement is identical to the case of 0 broken bars. The MCSA spectra near f_s are shown in Fig. 9(a)-(c) for 0, 1, and 2 adjacent broken bars, and in Fig. 9(d) for 2 non-adjacent broken bars. It can be seen that the f_{brb} component of MCSA also increases with the severity of adjacent broken bars, but cannot be observed for the case of non-adjacent broken bars. The results of Fig. 9 also show that the 4x slip frequency

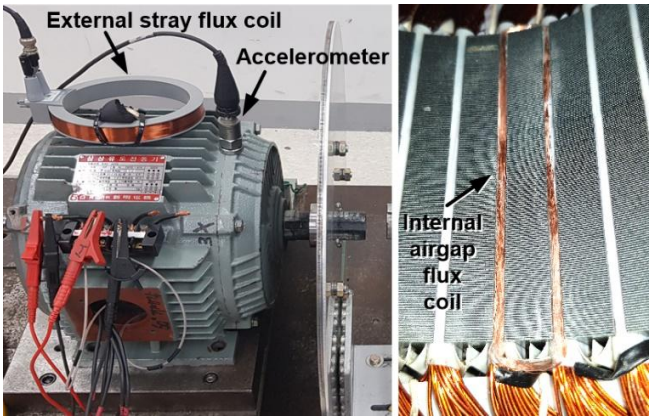

(a) (b)

Fig. 7. Experimental setup: 380 V, 7.5 hp, 4 pole induction motor with (a) external stray flux and (b) internal airgap flux search coils.

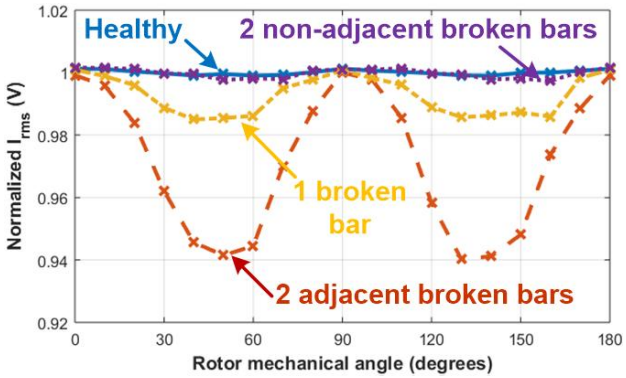

Fig. 8. Experimental results of off-line single phase rotation test: normalized I_{rms} vs. rotor position for 0, 1, 2 adjacent broken bars and 2 non-adjacent broken bars separated by 90 electrical degrees.

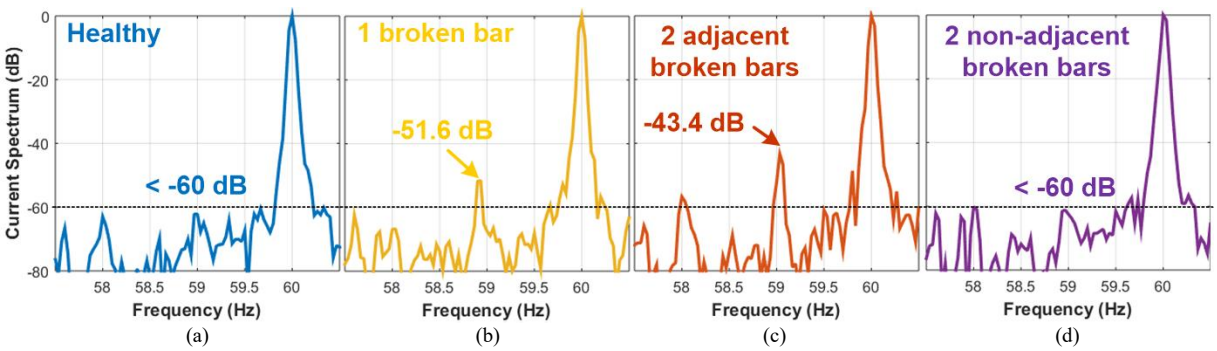

(a) (b) (c) (d)

Fig. 9. Experimental results: f_{brb} component in stator current spectra (MCSA) for (a) 0, (b) 1, (c) 2 adjacent, and (d) 2 non-adjacent broken bars.

sideband components produced by the secondary local saturation proposed in [16] cannot be applied for detecting non-adjacent broken bars. The STFT time-frequency plots of the f_{brb} component for the 4 cases are shown in Fig. 10. The f_{brb} component resembles a V pattern that starts at 60 Hz, decreases to 0 Hz, and increases to 60 Hz during the start as s decreases from 1 to 0, as can be seen in (1) and demonstrated in [3], [6], [10]-[13]. The results show that the intensity level of the V pattern increases up to 2 adjacent broken bars, but decreases to the inherent asymmetry level for 2 broken bars 90° apart. The results of Figs. 8-10 clearly show that the conventional electrical tests used in the field cannot be applied for detecting non-adjacent broken bars.

The external stray flux spectra that show the f_{rrf} and sf_s components for the 4 rotors are shown in Figs. 11-12, respectively. It can be seen in Fig. 11 that the proposed f_{rrf} component increases with broken bars for all cases including the 2 non-adjacent broken bars. The inherent level of f_{rrf} at 41.8 dB increased with the number of broken bars, where the increase was approximately 2x of the inherent value (6 dB) for 2 adjacent and non-adjacent broken bars. This is meaningful considering that the 2 non-adjacent broken bars could not be detected by all electrical tests shown in Figs. 8-10. It can be seen in Fig. 12 that the sf_s component does not always serve as a reliable indicator, as it is small and does not increase with the severity of broken bars. The $3sf_s$ components do increase with broken bar severity in Fig. 12, but is below -70 dB (<0.03% of the fundamental frequency), and require further investigation as they are produced by the sf_s components. The STFT plot of the external stray flux measured during motor starting is shown in Fig. 13 with the sf_s and f_{rrf} components highlighted. It can be seen that the intensity of the sf_s component is not consistent with the fault severity as in steady state (Fig. 12), and the $3sf_s$ component could not be clearly observed for all faulty cases during the starting transient. This shows that the sf_s and $3sf_s$ components cannot serve as reliable rotor fault indicators during both steady state and starting transient.

The internal airgap flux spectra of the f_{rrf} components is

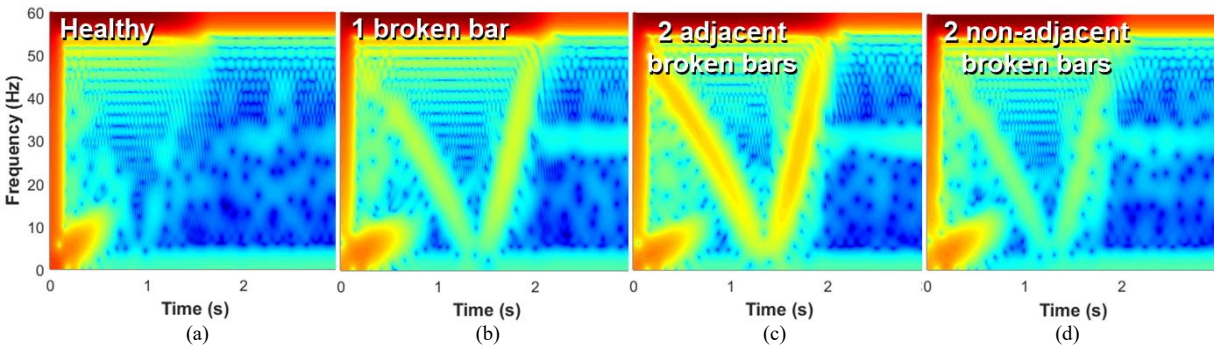

Fig. 10. Experimental results: f_{brb} component in STFT plot of stator current during starting transient for (a) 0, (b) 1, (c) 2 adjacent, and (d) 2 non-adjacent broken bars.

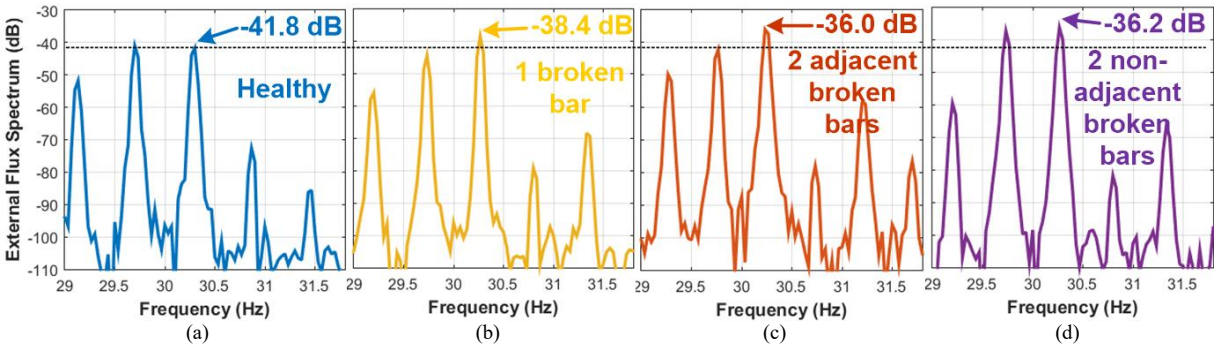

Fig. 11. Experimental results: f_{rrf} component in external stray flux spectra for (a) 0, (b) 1, (c) 2 adjacent, and (d) 2 non-adjacent broken bars.

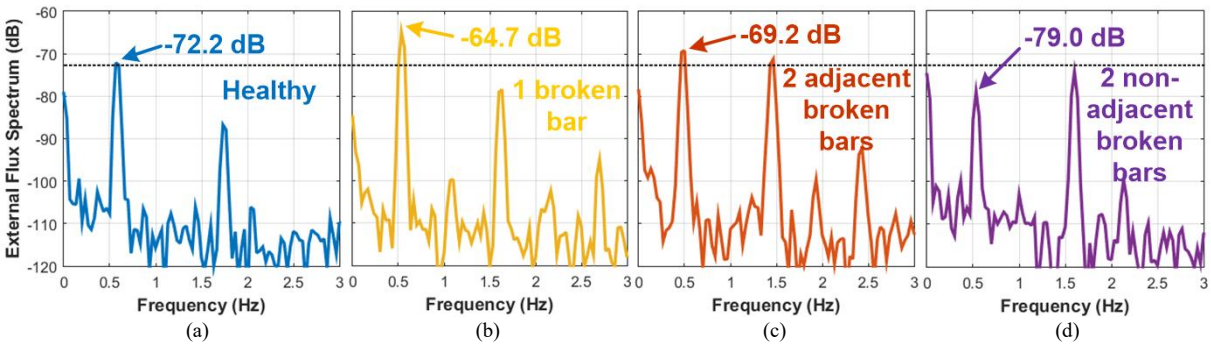

Fig. 12. Experimental results: sf_s and $3sf_s$ components in external stray flux spectra for (a) 0, (b) 1, (c) 2 adjacent, and (d) 2 non-adjacent broken bars.

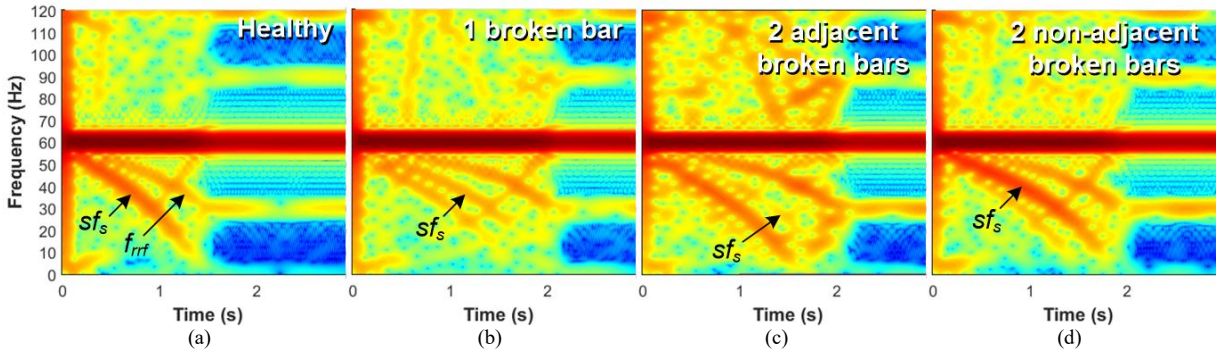

(a) (b) (c) (d)

Fig. 13. Experimental results: sf_s and f_{rrf} components in STFT plot of external stray flux during starting transient for (a) 0, (b) 1, (c) 2 adjacent, and (d) 2 non-adjacent broken bars.

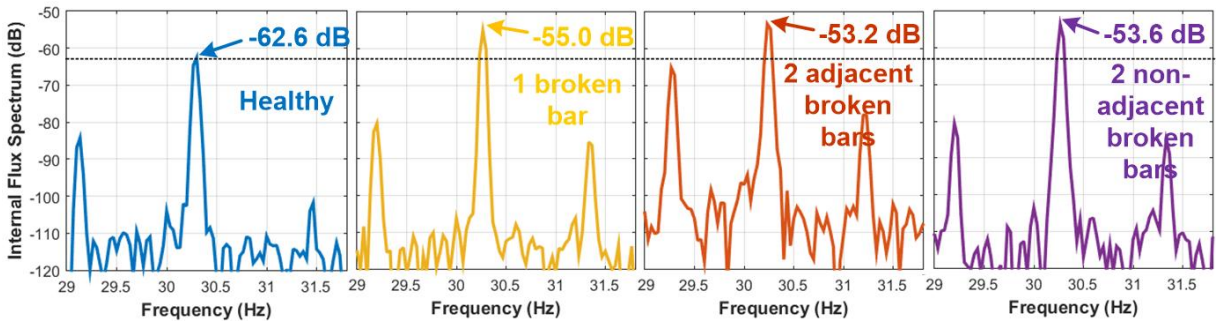

(a) (b) (c) (d)

Fig. 14. Experimental results: f_{rrf} component in internal airgap flux spectra for (a) 0, (b) 1, (c) 2 adjacent, and (d) 2 non-adjacent broken bars.

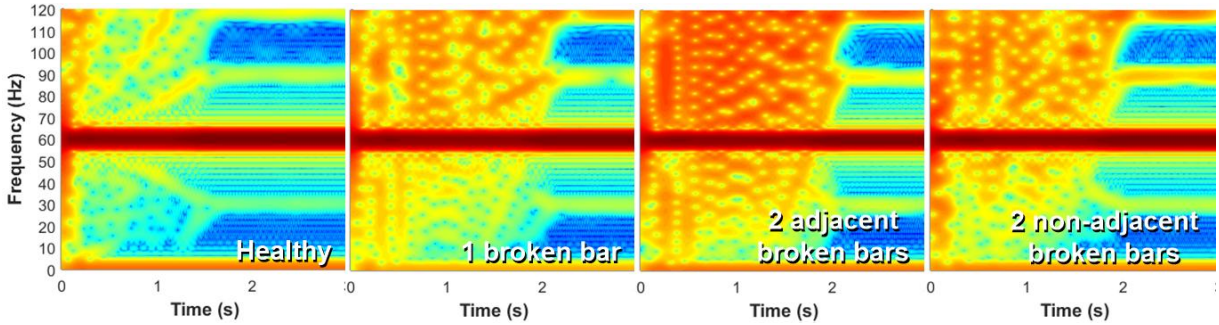

(a) (b) (c) (d)

Fig. 15. Experimental results: f_{rrf} components in STFT plot of internal airgap flux during starting transient for (a) 0, (b) 1, (c) 2 adjacent, and (d) 2 non-adjacent broken bars.

shown in Fig. 14 for the 4 cases. It can be seen that the proposed fault indicator increases with broken bar severity regardless of whether the broken bars are adjacent or non-adjacent. When compared to the external flux, the inherent f_{rrf} component is smaller and the increase in dB level is larger making it a more reliable indicator. The STFT time-frequency plot of the internal airgap flux during the starting transient is shown in Fig. 15. The increase in the magnitude of the integer multiples of the f_r sidebands of the f_s and $3f_s$ components between 0 and 120 Hz can be clearly observed when broken rotor bars are present, as predicted Fig. 6. The steep drop in the current of the slots with broken bars produces the strong f_r sidebands in the airgap flux, as predicted. The comparative test results of the 4 cases in Figs. 8-15 show that flux monitoring can provide detection of non-adjacent broken bars for cases where existing electrical tests fail. The reliability of using the internal airgap flux is superior, especially during the starting transient.

To show that the f_{rrf} sideband of the internal and external flux is sensitive to broken bars while not being sensitive to external load interference, testing was performed under severe mechanical load unbalance conditions. Bolts were added to the disc in Fig. 7(a) to produce "unacceptable" vibration levels above 7.1 mm/sec according to ISO10816 [46]. The test results of the f_{rrf} component for stator current, external stray and internal airgap flux, and vibration (velocity) are shown in Fig. 16. It can be seen that mechanical load unbalance that produces "unacceptable" level of vibration of 10.3 mm/sec (Fig 16(d)) and 28.6 dB increase in MCSA (Fig. 16(a)) does not cause any noticeable change in the f_{rrf} components of the external and internal flux (Figs. 16(b)-(c)). This makes the proposed f_{rrf} component a reliable indicator of broken bar faults.

V. Conclusion

Electrically symmetrical non-adjacent broken bars cannot be detected by any commercial electrical test method, and can

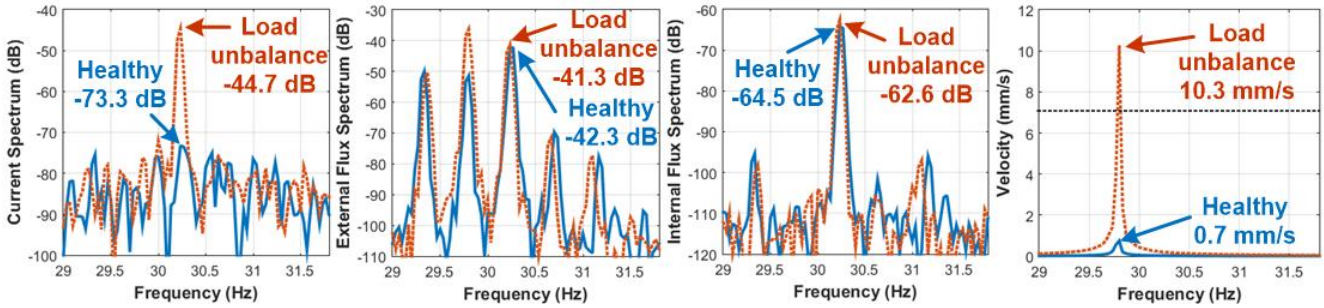

Fig. 16. Experimental results: f_{rrf} component for motor with and without mechanical load unbalance in the spectra of (a) stator current, (b) external stray flux, (c) internal airgap flux, and (d) vibration (velocity).

lead to a forced outage of the motor without prior warning. In this paper, analysis of external stray flux and airgap flux measurements was investigated as a means of detecting broken bars regardless of their relative position. Monitoring of the rotor rotational frequency sidebands of the supply frequency and odd harmonics was proposed as an indicator for detecting of broken bars. It was shown that the abrupt drop in the current in the rotor slot with the broken bar enables detection of both adjacent and non-adjacent broken bars with the search coil measurement. Experimental test results showed that the proposed method can be used for reliable detection of rotor faults under steady state or starting transient. It was shown that the reliability of the internal airgap flux measurement is superior to external stray flux, especially if the flux is analyzed during the starting transient. The proposed method is expected to provide reliable detection of non-adjacent broken bars that could not be detected by any electrical test method.

ACKNOWELDGMENT

This work was supported by the National Research Foundation of Korea(NRF) grant funded by the Korea government(MSIT) under Grant NRF-2019R1A2C1084104

REFERENCES

[1] A. H. Bonnett, and T. Albers, "Squirrel-cage rotor options for AC induction motors," *IEEE Trans. on Ind. Appl.*, vol. 37, no. 4, pp. 1197-1209, July/Aug. 2001.

[2] M. Hodowanec, and W.R. Finley, "Copper versus aluminum-which construction is best? [induction motor rotors]," *IEEE Ind. Appl. Mag.*, vol. 8, no. 4, pp. 14-25, Jul./Aug. 2002.

[3] C. Yang *et al*., "Starting current analysis for condition monitoring of medium voltage induction motors in the steel industry," *Proc. of* IEEE *Ind. Appl. Soc. Annu. Meet.*, pp. 1-9, 2017.

[4] T. Bishop, "Squirrel cage rotor testing," *EASA Convention*, 2003.

[5] G.C. Stone, I. Culbert, E.A. Boulter, H. Dhirani, *Electrical insulation for rotating machines – design, evaluation, aging, testing, and repair*, IEEE Press Series on Power Engineering, John Wiley and Sons, 2014.

[6] S. Lee, et al., "Identification of false rotor fault indications produced by on-line MCSA for medium voltage induction machines," *IEEE Trans. Ind. Appl.*, vol. 52, no.1, pp. 729-738, Jan./Feb. 2016.

[7] C. Hargis, et al., "The detection of rotor defects in induction motors," *Proc. IEE ICEMDA*, pp. 216-220, 1982.

[8] W.T. Thomson, "On-line current monitoring – the influence of mechanical loads or a unique rotor design on the diagnosis of broken rotor bars in induction motors," *Proc. of ICEM*, pp. 1236-1240, 1992.

[9] A. Bellini, *et al.*, "On-field experience with on-line diagnosis of large induction motors cage failures using MCSA," *IEEE Trans. on Ind. Appl.*, pp. 1045-1053, vol. 38, no. 4, July/Aug. 2002.

[10] C. Yang, *et al.*, "Reliable detection of induction motor rotor faults under the rotor axial air duct influence," *IEEE Trans. on Ind. Appl.*, vol. 50, no. 4, July/Aug. 2014.

[11] J. Antonino-Daviu, *et al.*, "Detection of broken outer cage bars for double cage induction motors under the startup transient," *IEEE Trans. on Ind. Appl.*, vol. 48, no. 5, pp. 1539-1548, Sept./Oct. 2012.

[12] Y. Park, M. Jeong, S.B. Lee, J.A. Antonino-Daviu, M. Teska, "Influence of blade pass frequency vibrations on MCSA-based rotor fault detection of induction motors," *IEEE Trans. on Ind. Appl.*, vol. 53, no. 3, May/June 2017.

[13] H. Kim, S.B. Lee, S.B. Park, S.H. Kia, and G.A. Capolino, "Reliable detection of rotor faults under the influence of low frequency load torque oscillations for applications with speed reduction couplings," *IEEE Trans. on Ind. Appl.*, vol. 52, no.2, pp. 1460-1468, Mar./Apr. 2016.

[14] T.J. Sobczyk, W. Maciolek, "Diagnostics of rotor-cage faults supported by effects due to higher MMF harmonics," *Proc. of Power Tech. Conf.*, vol. 2, pp. 5-9, June 2003.

[15] M. Riera-Guasp, J. Pons-Llinares, F. Vedreño-Santos, J.A. Antonino-Daviu, M. Fernández Cabanas, "Evaluation of the amplitudes of high-order fault related components in double bar faults," *Proc. of IEEE SDEMPED*, pp. 307-315, 2011.

[16] G.Y. Sizov, A. Sayed-Ahmed, C. Yeh, N.A.O. Demerdash, "Analysis and diagnostics of adjacent and nonadjacent broken-rotor-bar faults in squirrel-cage induction machines," *IEEE Trans. Ind. Electron.*, vol. 56, no. 11, pp. 4627-4641, Nov. 2009.

[17] M. Riera-Guasp, *et al.*, "Influence of nonconsecutive bar breakages in motor current signature analysis for the diagnosis of rotor faults in induction motors," *IEEE Trans. Energy Convers.*, vol. 25, no. 1, pp. 80-89, March 2010.

[18] C. Kral, H. Kapeller, J.V. Gragger, A. Haumer, B. Kubicek, "Phenomenon rotor fault-multiple electrical rotor asymmetries in induction machines," *IEEE Trans. Power Electron.*, vol. 25, no. 5, pp. 1124-1134, May 2010.

[19] M.E.H. Benbouzid, "A review of induction motors signature analysis as a medium for faults detection," *IEEE Trans. Ind. Electr.*, vol. 47, no. 5, pp. 984-993, Oct. 2000.

[20] T. J. Sobczyk and W. Maciolek, "Does the component $(1-2s)f_0$ in stator currents is sufficient for detection of rotor cage faults?," *Proc. of IEEE SDEMPED*, pp. 1-5 2005.

[21] J.A. Antonino-Daviu, K.N. Gyftakis, R. Garcia-Hernandez, H. Razik, A.J.M. Cardoso, "Comparative influence of adjacent and non-adjacent broken rotor bars on the induction motor diagnosis through MCSA and ZSC methods," *Proc.of IECON*, pp. 1680-1685, 2015.

[22] K. N. Gyftakis, J. A. Antonino-Daviu and A. J. M. Cardoso, "A reliable indicator to detect non-adjacent broken rotor bars severity in induction motors," *Proc. of ICEM*,, pp. 2910-2916, 2016.

[23] P. A. Panagiotou, I. Arvanitakis, N. Lophitis, J. Antonino-Daviu and K. N. Gyftakis, "A New Approach for Broken Rotor Bar Detection in Induction Motors Using Frequency Extraction in Stray Flux Signals," *Early access article, IEEE Transactions on Industry Applications*.

[24] J. Antonino-Daviu, H. Razik, A. Quijano-Lopez and V. Climente-Alarcon, "Detection of rotor faults via transient analysis of the external magnetic field," *Proc. IECON*, pp. 3815-3821, 2017.

[25] M. S. Erlicki, Y. Porat, A. Alexandrovitz, "Leakage field changes of an induction motor as indication of nonsymmetric supply," *IEEE Trans. Ind. Gen. Appl.*, vol. IGA-7, no. 6, pp. 713-717, Nov. 1971.

[26] Peter Vas, "Parameter estimation, condition monitoring, and diagnosis of electrical machines," Clarendon Press, Oxford Science Publications, UK 1993.

[27] J. Penman, M. N. Dey, A. J. Tait, W. E. Bryan, "Condition monitoring of electrical drives," *IEE Proc. B – Electr. Power Appl.*, vol. 133, no. 3, pp. 142-148, May 1986.

[28] N.M. Elkasabgy, A.R. Eastham, G.E. Dawson, "Detection of broken bars in the cage rotor on an induction machine," *IEEE Trans. Ind. Appl.*, vol. 28, no. 1, pp. 165-171, Jan./Feb. 1992.

[29] V. Kokko, "Condition monitoring of squirrel-cage motors by axial magnetic field measurements," Univ. of Oulu, 2003.

[30] H. Henao, C. Demian, G.A. Capolino, "A frequency-domain detection of stator winding faults in induction machines using an external flux sensor," *IEEE Trans. Ind. Appl.*, vol. 39, no. 5, pp. 1272-1279, Sept./Oct. 2003.

[31] C. Concari, G. Franceschini, C. Tassoni, "Differential diagnosis based on multivariable monitoring to assess induction machine rotor conditions," *IEEE Trans. Ind. Electron.*, vol. 55, no. 12, pp. 4156-4166, Dec. 2008.

[32] R. Romary, S. Jelassi, J.F. Brudny, "Stator-interlaminar-fault detection using an external-flux-density sensor," *IEEE Trans. Ind. Electron.*, vol. 57, no. 1, pp. 237-243, Jan. 2010.

[33] A. Ceban, R. Pusca, R. Romary, "Study of rotor faults in induction motors using external magnetic field analysis," *IEEE Trans. Ind. Electron.*, vol. 59, no. 5, pp. 2082-2093, May 2012.

[34] J. A. Ramirez-Nunez *et al*., "Evaluation of the detectability of electromechanical faults in induction motors via transient analysis of the stray flux," *IEEE Trans. Ind. Appl.*, vol. 54, no. 5, pp. 4324-4332, Sept.-Oct. 2018.

[35] L. Frosini, C. Harlişca, L. Szabó, "Induction machine bearing fault detection by means of statistical processing of the stray flux measurement," *IEEE Trans. Ind. Electron.*, vol. 62, no. 3, pp. 1846-1854, Mar. 2015.

[36] O. Vitek, M. Janda, V. Hajek, P. Bauer, "Detection of eccentricity and bearings fault using stray flux monitoring," *Proc. of IEEE SDEMPED*, pp. 456-461, 2011.

[37] G. Mirzaeva, K.I. Saad, M.G. Jahromi, "Comprehensive diagnostics of induction motor faults based on measurement of space and time dependencies of air gap flux," *IEEE Trans. Ind. Appl.*, vol. 53, no. 3, pp. 2657-2666, May/June 2017.

[38] J. Yun *et al*., "Airgap search coil-based detection of damper bar failures in salient pole synchronous motors," *IEEE Trans. Ind. Appl*., vol. 55, no. 4, pp. 3640-3648, July/Aug. 2019.

[39] M.F. Cabanas, *et al*., "A new portable, self-powered, and wireless instrument for the early detection of broken rotor bars in induction motors," *IEEE Trans. Ind. Electron.*, vol. 58, no. 10, pp. 4917-4930, Oct. 2011.

[40] T. Goktas, M. Arkan, M.S. Mamis, B. Akin, "Separation of induction motor rotor faults and low frequency load oscillations through the radial leakage flux," *Proc. of IEEE ECCE*, pp. 3165-3170, Oct. 2017.

[41] Y. Park *et al*., "Stray Flux Monitoring for Reliable Detection of Rotor Faults Under the Influence of Rotor Axial Air Ducts," *IEEE Trans. Ind. Electron.*, vol. 66, no. 10, pp. 7561-7570, Oct. 2019.

[42] ABB (2018), *ABB Ability Smart Sensor for motors*, [Online]. Available: https://new.abb.com/motors-generators/service/advanced-services/smart-sensor/smart-sensor-for-motors.

[43] WEG Motor Group, *WEG Motor Scan – whitepaper,* [Online]. Available: https://www.weg.net/wegmotorscan/en.

[44] Y. Park, H. Choi, S.B. Lee, K. Gyftakis, "Flux-based detection of non-adjacent rotor bar damage in squirrel cage induction motors, *Proc. of ECCE*, pp. 7019-7026, Sept. 2019.

[45] L. Cohen, *Time-frequency analysis*. A.V. Oppenheim, Ed. Prentice Hall Signal Processing Series, New Jersey, 1995.

[46] *Mechanical vibration - evaluation of machine vibration by measurements on non-rotating parts - part 3: Industrial machines with nominal power above 15 kW and nominal speeds between 120 r/min and 15 000 r/min when measured in situ*, ISO 10816-3, 2009.